euspen's 22nd International Conference & Exhibition, Geneva, CH, May/June 2022
www.euspen.eu

CT-based traceable interface area detection in Al7075-T6 adhesive bonded structures

I. Holgado[1]; N. Ortega[2]; B. Perez[3]; S. Florez[3]; S. Plaza[2]

[1] *Aeronautics Advanced Manufacturing Center (CFAA), Parque tecnológico de Bizkaia, 202, 48170 Zamudio, Spain*
[2] *Department of Mechanical Engineering, Faculty of Engineering of Bilbao, Plaza Ingeniero Torres Quevedo 1, 48013 Bilbao, Spain*
[3] *TECNALIA Research and Innovation - Basque Research and Technology Alliance (BRTA), Parque Científico y Tecnológico de Gipuzkoa, Mikeletegi Pasealekua 2, 20009 Donostia-San Sebastián/Spain*

Ibon.holgado@ehu.eus

Abstract

In emerging technologies such as aerospace and aeronautics the joining of multi-material parts is a growing need for the development of components with improved properties. Among efficient joining technologies, adhesive bonding is considered an optimal method for joining multi-material structures, however, its use is limited due to inadequate evaluation of bond quality by non-destructive testing (NDT) methods. Recently, computed tomography (CT) is becoming more and more accepted in the non-destructive testing (NDT) community, thanks to the equipment and software development. This technology is capable of performing quantitative dimensional and geometric analysis, for example of adhesive bonds. Nevertheless, quantitative results obtained by CT are strongly influenced by a large number of error sources and thus the accuracy of CT-based measurements remains yet largely uncertain. In most cases a consistent methodology is needed, so that CT could be considered a reliable technology. This paper aims to evaluate the adhesive bonding quality in metal bonded structures by means of CT. To do so, a structural adhesives with four different Aluminum specimens are analyzed. The adhesives used are MERBENIT SF50® and BETAMATE 2810® and the substrates of Al7075-T6 of 3mm thickness. For each bonding configuration, a novel ML–based method for the detection of the contact area between adhesive and substrate is provided. Each adhesive interface area measurement is associated with its corresponding task-specific uncertainty estimation. Results are promising and useful for adhesive bond quality evaluations in CT equipment.

Adhesive, Computed tomography, Non-destructive testing, Uncertainty

1. Introduction

The use of lightweight aluminium (Al) alloys and composites has increased dramatically both to meet environmental requirements and to improve the performance of emerging technology vehicles [1]. Efficient joining technologies for these materials are, however, a challenge due to their different natures.

Budhe et al. [2] indicate that adhesive bonding is considered an optimal method for joining multi-material structures. Adhesively bonded structures not only create a high strength-to-weight ratio, but also allow for homogeneous load distribution.

In spite of its potential advantages, the use of adhesives in safety product structures is limited due to inadequate evaluation of bonding quality by non-destructive testing methods [3]. Ideally, the adhesive volume should be uniform and free of voids. Unfortunately, as the liquid adhesive contains water that evaporates during the curing phase (along with other physical effects), the defects shown in figure 1 can occur in the cured adhesive layer.

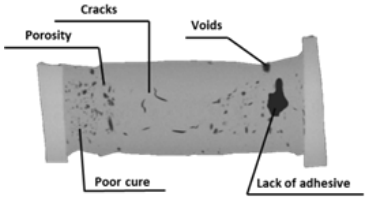

Figure 1. Adhesive bond cross section with common defects.

Despite numerous studies on qualitative inspection methods for such joints, the limitation of accurately assessing the joint interface area is a challenge that only a few of them have addressed [3].

1.1 Adhesive joint inspection

There are numerous inspection technologies to evaluate the adhesive joints quality. This inspection techniques can be classified as destructive (DT) and non-desctructive testing methods (NDT). Destructive inspection methods require to manufacture test parts which become in an indirect data about the internal integrity of the actual joined components. To overcome the inspection limitations and to meet safety requirements, reliable non-destructive testing methods are essential to first detect and then accurately measure defects associated with the bonding process.

A number of studies have discussed the evaluation of bonding quality with various non-destructive testing (NDT) methods, being ultrasound and thermography techniques the most used ones. However, recently, computed tomography (CT) is becoming more and more accepted in the non-destructive testing (NDT) community, thanks to the equipment and software development. In comparison with other NDT techniques, CT imaging techniques can provide increased spatial resolution and can inspect the full thickness of the adhesive quantitatively [4]. Nonetheless, CT measurements values are strongly influenced by a high number of error sources and thus the accuracy and reproducibility of CT-based measurements remains yet largely uncertain. Despite the current challenges, CT measurements

uncertainty estimates are esential for different measurement technology comparisons and acceptance of the results[5]. Over the last two decades, the substitution method has been generally applied for the estimation of CT based measurements uncertainties. This empirical approach is based on repeated measurements carried out on a calibrated standard similar in thickness and material to the component under study [6].

1.2. CT image segmentation and CT measurement uncertainty

CT imaging technology involves numerous applications such as metrological tasks, reverse engineering and 3D image-based simulations. In all these applications, the first step is image segmentation, which usually consists of identifying the boundaries of the surface of each present class (or only between a material and the background) of both external and internal features [7].

For this process, traditional image segmentation approaches involve manual segmentation, where a technician applies different procedures for determining the surface location, typically by global or local thresholding. However, manual segmentation is fraught with irreproducibility and variability from person to person. Although the existing tools themselves (e.g. VGSTudio advanced surface determination , Valley or Otsu thresholding algorithms) are consistent, chances are that even two qualified technician performing segmentation on the same CT data will result in different segmentations leading to different measurement results. As a rule of thumb, the goal of the technician performing the segmentation is to adjust the result to what the human eye can see, so it is a completely subjective method, which never end as the most correct segmentation [8].

The range of possible segmentations, considering all the variables influencing the process, represents the uncertainty of the segmentation process. The correct segmentation, however, may or may not lie within this zone, and the systematic error between the calibrated reference value and the segmentation result is considered as the bias. Therefore, the bias itseld needs to be considered separately from uncertainty but together with the result. Standard uncertainty due to the reference values measurement (u_{cal}), Standard uncertainty of CT measurement process (u_{rep}) (once the voxel size has been calibrated), segmentation uncertainty (u_{seg}) and bias (b) are considered in this work as the total expanded uncertainty contributors, equation 1. The standard uncertainty due to the drift (u_{drift}) and the standard uncertainty due to the variations in material (u_w) are considered as negligible.

$$U_{MP} = k \cdot \sqrt{u_{cal}^2 + u_p^2 + u_{seg}^2 + b^2} \quad (1)$$

Fortunately, the main disadvantages of manual segmentation can be overcome by machine learning (ML) techniques, which generate highly reproducible values, spare technicians labour-intensive tasks and can achieve values with high accuracy. In this study a novel ML procedure using a Random Forest (RF) classifier is applied.

This paper presents a methodology to automatically and accurately detect the adhesive/adhesive surface by CT . On the whole, it comes that the novelty of the present work is twofold: first, to investigate the adhesive surface interfacial contact by means of CT and applying ML–based RF algorithm. The proposed test configuration allows to reproduce at the macro-scale the adhesive surface integrity and same methology holds promise for application in micro-scale resolution CT systems. Second, a novel uncertainty assessment of the proposed method is provided, thus, the methodology is consistent for a faithful comparison, reproducibility and reliability of CT measurement results.

2. Materials and methods

The dimensions and details of the inspected specimens, with single lap geometry, are shown in figure 2. The substrates material is Aluminium 7075-T6, and two different adhesives were used, a flexible adhesive MERBENIT SF50® and a rigid adhesive ARALDITE 2012®.

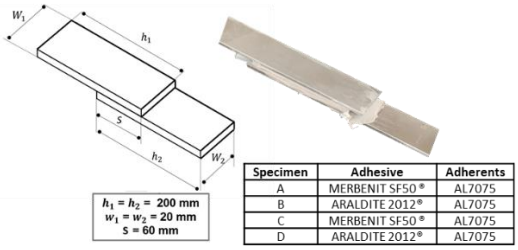

Specimen	Adhesive	Adherents
A	MERBENIT SF50 ®	AL7075
B	ARALDITE 2012®	AL7075
C	MERBENIT SF50 ®	AL7075
D	ARALDITE 2012®	AL7075

Figure 2. Inspected specimens dimensions

For both cases, the surface treatment applied consisted of the following steps: cleaning surface with acetone, sanding (paper grit 80) and cleaning with acetone.

In order to be able to obtain the interface area reference values, it is necessary to have access to the interface area, e.g. by means of an optical system. Thus, to expose the interfaces, an adhesive failure mode is usually triggered at the bonding joints (a peel-off where no adhesive residue remains on the substrate). For that purpose, in this work a release agent (LOCTITE FREKOTE 55-NC) was applied on the Aluminium plates. Moreover, *Teflon* tabs were placed on one of the substrates, fixing with low thickness double-sided tape, in order to delimit the bonding area and act as a thickness controller of the adhesive layer which are applied on both substrates (for flexible adhesive 2mm, and for rigid one 1mm) and then the other substrate was placed. After removing the excess adhesive, a slight pressure was applied to ensure good contact. The adhesive curing was carried out in the laboratory, at a controlled conditions of temperature and humidity (25ºC-50%RH) for 24 hours, according to TDS.

All the specimens were imaged via X-ray computed tomography at a 89 µm resolution (voxel size). The research was done on a set of CT slices images sized 1063 × 1056 pixels coming from General Electric X-Cube Compact machine. The source voltage was selected to avoid the extinction of the X-ray beam in the most unfavourable position. Under this criteria, the voltage was adjusted to 150kV and then the tube current value was chosen to be high enough as it leads to a reduced exposure time, allowing the least scanning time without decreasing the image contrast/brightness. This resulted in 4mA and 100ms of exposure time. The combination of 1mm copper and 0.5mm tin filters achieved a homogenization effect of photons energy that reached to the workpiece, minimizing the beam hardening effect.

For adhesive segmentation, the figure 3 (ML)-based method was implemented.

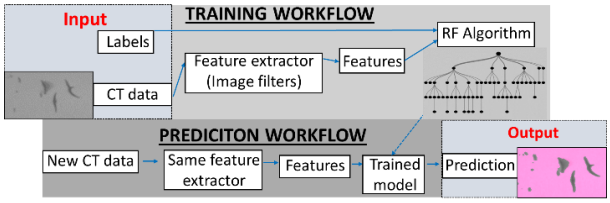

Figure 3. ML segmentation workflow

The setup phase for the training and prediction consisted of the following choices:

1) *Class labelling:* First, the learning process starts by manually labelling a particular CT image slice

(supervised learning) near the apparent interface. The labelling was carried out by APEER, a free cloud-based platform focused on image processing tasks [9]. Only the pixels that can be reliably identified as pores, adhesive or *Teflon* were labelled (unlabelling the uncertain contours), as shown in the figure 4.

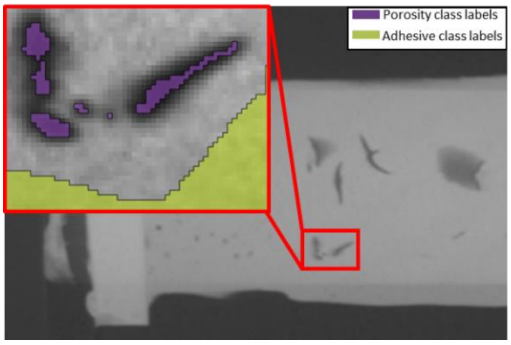

Figure 4. CT image labelling

2) *Features:* In image data, the features are the pixel values of digitally filtered images. In this study, 100 Contrast Limited Adaptive Histogram Equalization (CLAHE), 50 Fourier transforms mask , 2 Gaussian (sigma 3 and 7) and median image processing filters were applied for each pixel value features extraction, apart from the natural value of the original pixels. Each feature and the labels were used to train the RF model in order to predict the new input image labels.
3) *Random Forest (RF) algorithm:* RF classification algorithm implemented in python Scikit-learn library, version 1.0.2, was used for classification porpoises [10]. The RF algorithm combines classification results from several decision trees. First, some trees are constructed and fitted to the pixel values during the training , using a random subset of features to train each tree. Then the results of classification from each tree for each pixel are named as a class vote and the derived classification is determined by majority of class votes.
   In all decision trees, the first node corresponds to the original pixel value, the intermediate nodes to the features and the label value to the prediction.
   The number of stimators used were 100. More information about the algorithm can be found in [10].
4) *Predicition:* Once the RF model is created, the new images are predicted extracting the same features as in the previous ones.

To assure the traceability of the interface area measurement, the expanded uncertainty of the CT measurement process (U_{MP}) was determined. The presented task-specific uncertainty estimation was based on repeated area measurements carried out on each scanned metal/metal adhesive interfaces.

First, u_{cal} was estimated following [11]. For this purpose Alicona G4 InfiniteFocus® microscope was used under high repeatability conditions and with a vertical resolution of 10 nm and therefore, u_{cal} was considered as the standard uncertainty due to the Alicona measurement process. The uncertainty u_{cal} is given by the standard uncertainty associated with the calibration of the equipment used (u_E) and by the standard uncertainty associated with the repeatability of the reference values measurements (u_{rep}), equation 2:

$$u_{cal} = u_E + u_{rep} \quad (2)$$

The uncertainty component u_E was estimated by the extended standard uncertainty U_{cal} and the coverage factor (k_{cal}) stated in the calibration certificate of the calibrating equipment using equation (3):

$$u_E = \frac{U_{cal}}{k_{cal}} \quad (3)$$

The standard uncertainty associated with the repeatability of the reference values measurements (u_{rep}) was determined by by the standard deviation of 3 Alicona measurements (σ) and by the number of measurements (N):

$$u_{rep} = \sqrt{\frac{\sigma}{N}} \quad (4)$$

Then, to consider the repeatability of CT measurement results, 4 CT scans were replicated with identical set-up, following the procedure described in [12]. Thus u_p is considered as:

$$u_p = \sqrt{[\frac{1}{N-1} \cdot \sum_{i=1}^{N}(y_i - \bar{y})^2]} \quad (5)$$

The systematic errors (b) between the mean values of CT measurements (y) and the reference values (y_{cal}) is defined as:

$$b = \bar{y} - y_{cal} \quad (6)$$

Then the image segmentation uncertainty (u_{seg}) was estimated by the above mentioned 4 CT scans adhesive interface area segmentations. It is worth noting the novelty and necessity of assessing u_{seg} separately from b, as not all the reference values are included in the u_{seg} range.

Once the RF algorithm was trained, a prediction was made for all 4 CT image interfaces of each specimen described in the figure 3. As the precise interface is difficult to quantify, in each of the 4 repetitions a slightly different CT slice was defined as interface. This range was ±10 µm. Owing these slight differences, combined with the inherent lack of repeatability of the CT scanning process, the results of each segmentation differ slightly from each other repetitions. Therefore, in each segmentation of every repetition, certain pixels were considered as adhesive and other times not. According to this variability, all pixels that switched class in any of the 4 segmentations were marked within a new class, considered as a region of uncertainty. In the following figure 5 is shown one of the results as an example.

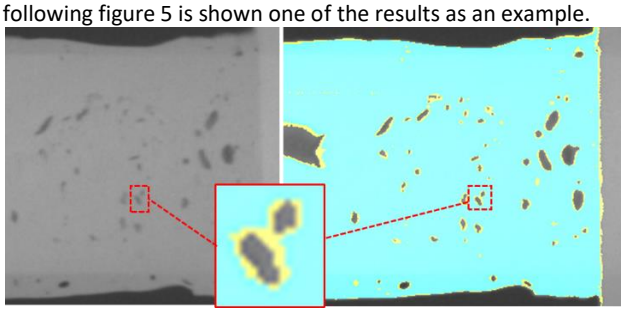

Figure 5. Specimen A segmentation uncertainty map example.

3. Results

Table 1 summarizes the results of the expanded uncertainties U_{MP} associated to the CT interface area measurement of each specimen.

Table 1 CT interface área measurements results.

	Specimens interface area according to figure 3			
	A	**B**	**C**	**D**
CT Interface area(mm^2)	1 348.660	991.525	1 270.403	1 315.662
U_{MP}(mm^2)	158.729	99.667	172.861	122.711
U_{MP}(%)	11.76%	10.05%	13.61%	9.33%

The figure 6 shows the uncertainty budget of the CT measurement process uncertainty assessment, strongly influenced by u_{seg} and b.

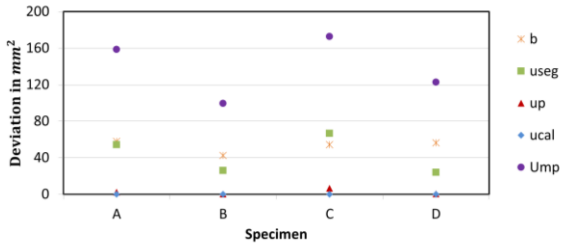

Figure 6. U_{MP} and uncertainty contributors values

From the results it can be concluded that CT measurements results were affected by high deviations due to the difference in resolution between the validation and CT equipment used. As a consequence of the relatively low resolution of the X-ray equipment, the unshaprness generated in CT images was such that defects of area less than 10 times the effective pixel area (0.89 μm^2) were highly overestimated by RF algorithm. Unfortunately, the studied adhesives contained a large amount of porosity and cracks of these dimensions, causing $\boldsymbol{U_{MP}}$ values up to 13.61% in CT interface area measurements. Larger area defects were less affected by equipment unsharpness, as shown in the segmentation uncertainty map in figure 5.

U_{MP} considered 2 differents effects, the irregular selection of different CT images as interfaces and the measurement of the adhesive area itself. In the case of MERBENIT SF50® flexible adhesives, the determination of the interface was much more problematic (due to its composition and structure), increasing the $\boldsymbol{u_{rep}}$ and b values, resulting in the highest $\boldsymbol{U_{MP}}$ values.

Considering the accuracy of the applied ML-based RF model, the results show a high correlation between the predicted values and the actual values. According to equation 7, the model accuracy was up to 0.99:

$$accuracy(y, \hat{y}) = \frac{1}{n_{pixel}} \sum_{i=0}^{n_{pixel}-1} 1(\hat{y}_i = y_i) \qquad (7)$$

Where $\hat{y}_i$ is the predicted value of the i-th sample and y_i is the corresponding true value. These methods are relatively more straightforward and accurate than the traditional laborious and time consuming manual segmentations. The main challenge to accurately segment these type of images is the wide range of grey numbers that are included in the same class, especially when feature sizes are variable, e.g. porosity.

5. Conclusions

From the research carried out the following conclusions can be drawn:

- A novel methodology to quantify image segmentation uncertainty using advanced ML-based algorithm was proposed. Segmentation uncertainty is needed, for example, for propagating uncertainty through image-based simulations. When u_{seg} is considered, realistic predicted physics quantities together with the respective uncertainty distributions can be provided and to date, this term stimation has received very little attention in the literature [8].

- Although the uncertainty values provided in the study are relatively high given the scanning resolution used, the CT measurement method has been shown to be repeatable. Even though it has not been demonstrated, applying this method to higher resolution CT images would be relatively straigthforward, which would greatly improve the $\boldsymbol{U_{MP}}$ values.

- The large amount of porosity with dimensions below 10 times the pixel size used, in the case of MERBENIT SF50® adhesives, leads to poorer accuracy in the measurements provided. In addition, due to the large grey diversity of each pore, the class segmentation is much more sensitive to labelling than in the case of ARALDITE 2012® adhesives.

Acknowledgements

Thanks are given to the Spanish Ministry of Science and Innovation for its support of the Research Project 'Investigation of a solution for the finishing and quality control of Aluminum aerospace components manufactured by SLM' (PID2020-118478RB-100).

References

[1] Birch S. Aluminium spaceframe technology. Automot Eng 1994;102(1):8–12.
[2] Budhe S, Banea MD, de Barros S, da Silva LFM. An updated review of adhesively bonded joints in composite materials. Int J Adhesion Adhes 2017;72:30–42. https://doi.org/10.1016/j.ijadhadh.2016.10.010.
[3] Yılmaz, B., & Jasiūnienė, E. (2020). Advanced ultrasonic NDT for weak bond detection in composite-adhesive bonded structures. International Journal of Adhesion and Adhesives, 102, 102675.
[4] Zheng, S., Vanderstelt, J., McDermid, J. R., & Kish, J. R. (2017). Non-destructive investigation of aluminum alloy hemmed joints using neutron radiography and X-ray computed tomography. NDT & E International, 91, 32-35.
[5] Villarraga-Gomez H, Thousand JD, Morse EP, Smith ST. CT measurements and their estimated uncertainty: the significance of temperature and bias determination. In: Proceedings of 15th international conference on metrology and properties of engineering surfaces. USA: University of North Carolina-Charlotte; 2015. p. 509–15.
[6] VDI/VDE 2630-2.1. Computed tomography in dimensional measurement –Determination of the uncertainty of measurement and the test process suitability of coordinate measurement systems with CT sensors. Berlin, Germany: The Association of German Engineers; 2013.
[7] Yagüe-Fabra, J. A., Ontiveros, S., Jiménez, R., Chitchian, S., Tosello, G., & Carmignato, S. (2013). A 3D edge detection technique for surface extraction in computed tomography for dimensional metrology applications. CIRP Annals, 62(1), 531-534.
[8] Krygier, M. C., LaBonte, T., Martinez, C., Norris, C., Sharma, K., Collins, L. N., ... & Roberts, S. A. (2021). Quantifying the unknown impact of segmentation uncertainty on image-based simulations. Nature communications, 12(1), 1-11.
[9] https://www.apeer.com/app/machine-learning/annotate ((accessed January 10, 2022)
[10] F. Pedregosa, G. Varoquaux, A. Gramfort, V. Michel, B. Thirion, O. Grisel, M. Blondel, P. Prettenhofer, R. Weiss, V. Dubourg, J. Vanderplas, A. Passos, D. Cournapeau, M. Brucher, M. Perrot, and E. Duchesnay. Scikit-learn: Machine learning in Python. JMLR, 12:2825–2830, 2011.
[11] Sładek, J. A. (2016). Coordinate metrology. Accuracy of Systems and Measurements.
[12] Ortega, N., Plaza, S., Pascual, A., Holgado, I., & Lamikiz, A. (2021). A methodology to obtain traceability for internal and external measurements of Inconel 718 components by means of XRCT. NDT & E International, 120, 102436.